Enhanced dispersoid precipitation and dispersion strengthening in an Al alloy by microalloying with Cd

Feng Qian[a], Shenbao Jin[b], Gang Sha[c], Yanjun Li[a,*]

[a] Department of Materials Science and Engineering, Norwegian University of Science and Technology, 7491, Trondheim, Norway

[b] Department of Materials Science and Engineering, Nanjing University of Science and Technology, 210094, Nanjing, China

[c] Herbert Gleiter Institute of Nanoscience, Nanjing University of Science and Technology, 210094, Nanjing, China

*Corresponding author. E-mail: yanjun.li@ntnu.no

Abstract

The dispersion hardening effect of Mn(Fe)-containing dispersoids in aluminium alloys has long been ignored since it is difficult to achieve a high number density of fine dispersoids with conventional alloying compositions. This work demonstrates a minor addition of Cd (0.05 at.%) can dramatically enhance the precipitation of α-Al(Mn,Fe)Si dispersoids and therefore the dispersion strengthening of AA3003 alloy. Similar to the 3003 base alloy, a peak hardness in the Cd-containing alloy was obtained after continuous heating to 450 °C. However, an improvement in yield strength by 25% was achieved by the Cd addition. Detailed transmission electron microscopy (TEM) and atom probe tomography (APT) investigations show that the Cd addition has changed the nucleation behaviour of α-Al(Mn,Fe)Si dispersoids from the conventional heterogeneous nucleation on dislocations to a more homogeneous manner. It is found that a high number density of Al-Cd nanoprecipitates formed during heating between 150 and 250 °C. These Al-Cd precipitates attracted Mn and Si atoms to form Mn,Si-rich clusters in/around them, which acted as the precursors for the later nucleation of α-Al(Mn,Fe)Si dispersoids at ~300 °C. As a result, the number density of dispersoids formed in the Cd-containing alloy after heating to 350-450 °C is about twice as that in the base alloy subjected

to the same heat treatment. This work proposes a new approach to enhance the nucleation of α-Al(Mn,Fe)Si dispersoids, which can help to further develop cheap Mn(Fe)-containing dispersoid-strengthened aluminium alloys for high-temperature applications.

Keywords: Precipitation; Dispersoid; Dispersion strengthening; Cadmium; Atom probe tomography

1 Introduction

The strength of age-hardenable aluminium alloys (e.g. 2xxx, 6xxx and 7xxx series) can be dramatically improved by the precipitation of (semi-)coherent precipitates upon artificial ageing treatment [1,2]. However, these strengthening precipitates are very sensitive to temperature. Due to coarsening, phase transformation and/or dissolution, they lose their strengthening effect at elevated temperatures. This makes it difficult for these ageing-hardening alloys to satisfy the increasing demands from automotive and aerospace industrial sectors for Al alloys that can sustain elevated service temperatures (≥ 250 °C). It has been demonstrated that an addition of individual or a combination of Zr, Sc and Er elements in aluminium alloys can introduce thermally stable, high-density, nano-sized dispersoids, such as Al_3Zr, Al_3Er, $Al_3(Zr_xSc_{1-x})$ [3,4,13–16,5–12]. As a result, the strength of the alloy at room temperature and especially at elevated temperatures can be largely increased [5,11,12]. Among these alloying elements, the effect of Sc is much more significant than that of other elements. However, the application of Sc-containing Al alloys has largely suffered from the extremely high price of Sc.

With a comparable thermal stability to the expensive Sc-containing dispersoids, the nano-sized Mn(Fe)-containing dispersoids have the potential to be developed as a cheaper solution for designing high-temperature Al alloys [17,18]. AA3xxx and some Mn-containing 5xxx and 6xxx Al alloys are normally supersaturated with Mn in the as-cast state [19–21]. During heating, the decomposition of the supersaturated solid solution (SSSS) will lead to the precipitation of different types of Mn(Fe)-containing dispersoids depending on the alloy composition and heat treatment process [19,20,22–24].

α-Al(Mn,Fe)Si is the most common dispersoid formed in these alloys, which has a cubic crystal structure and a lattice constant of a = 1.256 ~ 1.265 nm [25,26]. It is partially coherent and has a preferential orientation relationship (OR) with the Al matrix: $\{5\bar{2}\bar{7}\}_p \parallel \{011\}_m, < 1\bar{1}1 >_p \parallel$

$< 1\bar{1}1 >_m$ [19,27], where the subsript *p* and *m* represent particle and matrix, respectively. Li and Arnberg [24] reported that during the continuous heating of as-cast 3xxx alloys at a rate of 50 °C/h, α-Al(Mn,Fe)Si dispersoids started to precipitate at temperatures above 300 °C. While at temperatures higher than 500 °C, the size of dipsersoids grew fast and the number density reduced sharply with temperature due to the coarsening and disolution of α-dispersoids in the Al matrix.

Al_6(Mn,Fe), as another common type of dispersoids, usually precipitates in 3xxx alloys with a very low Si content and 5xxx alloys at higher temperatures during heat treatment, accompanying with the dissolution of α-dispersoids [20,23]. Al_6(Mn,Fe) dispersoids have an orthorhombic crystal structure and preferentially a platelet or long lath morphology with their habit planes coherent with the Al matrix. The most common OR between Al_6(Mn,Fe) and the Al matrix is determined as $(001)_p \parallel (3\bar{1}5)_m, [\bar{1}10]_p \parallel [21\bar{1}]_m$ [20]. Al_6(Mn,Fe) dispersoids are very stable at high temperatures and can survive even after a long-time soaking (600 °C, 24 h) [19,22]. However, the number density of Al_6(Mn,Fe) dispersoids is rather low while their size is much larger than α-Al(Mn,Fe)Si dispersoids.

Although a relatively high density of dispersoids can be obtained in 3xxx alloys during heating due to the higher Mn contents than 5xxx and 6xxx alloys, the number density of Mn(Fe)-containing dispersoids is still not high enough to achieve a distinct dispersion hardening effect. Instead, these dispersoids are more recognized for their significant effects on retarding recovery, recrystallization and grain growth [28–32]. In recent years, the dispersion hardening effect of Mn(Fe)-containing dispersoids has been re-assessed. It is found that a proper heat treatment can produce a higher number density of nano-sized α-Al(Mn,Fe)Si dispersoids and therefore a significant dispersion hardening [17–19,27,33–35]. For example, by an isothermal annealing at 375 °C for 24 h, the yield strength of AA3003 alloy could be increased by 53.8% in

comparison to the as-homogenized sample (600 °C, 24 h) [19]. To further improve the dispersion hardening effect of dispersoids, great efforts have been made on modifications of the chemical compositions of 3xxx alloys. It shows that increasing Mn, Si or Fe contents can effectively increase the number density of α-Al(Mn,Fe)Si dispersoids in 3xxx alloys [33,35]. Nevertheless, the current achievements in the dispersion strengthening of Mn-containing dispersoids are still not satisfactory, especially when compared to the Sc-containing alloys. This is attributed to the nucleation mechanism of Mn-containing dispersoids: most of them heterogeneously nucleate on dislocations [36–38] or on coarse Mg_2Si precipitates in Mg-containing alloys [37], which results in a low density and heterogeneous distribution of dispersoids.

Microalloying has been a widely used approach to modify the precipitation behaviour of nano-sized strengthening precipitates and therefore improve the mechanical properties of age-hardenable alloys. Additions of alloying elements, such as Cd [39–43], In [39,40], Sn [39,40,44–46] or Ag [42] in Al-Cu alloys and Cu [47–49], Ge [50], Ag [49] or Sn [51] in Al-Mg-Si alloys, have been demonstrated to enhance the age hardening effect of alloys. However, the underlying mechanisms are different depending on the microalloying elements and alloy compositions. Moreover, the mechanisms of some microalloying elements are rather complex and are still under debate. For example, several hypotheses have been proposed to interpret the mechanisms of impurity element Cd, In and Sn (here all referred to as X) in strengthening Al-Cu alloys. One hypothesis based on resistivity and dilatometer examinations on the early ageing stage suggested the enhanced nucleation of *θ'* is due to the fast coalescence of X-Cu-vacancy clusters [52,53]. The strong binding energy of X atoms with vacancies favours this proposal but it lacks direct experimental evidence. The second proposed mechanism is that the segregation of X atoms at the *θ'*/*α*-matrix interface reduces the interfacial energy of *θ'* nuclei [40,54–56]. This hypothesis which was initially proposed based on calorimetric measurements

and electron diffraction analyses also lack direct experimental supports. Another possible mechanism is that the prior precipitation of X atoms leads to the heterogeneous nucleation of *θ'* on them [39,56]. Careful APT and high-resolution TEM investigations on Al-Cu-Sn alloys by Ringer and Homma et al. [45,46] supported this mechanism. Such a mechanism has also been applied to explain the enhanced precipitation in Al-Cu alloys microalloyed with Si-Ge [57,58] and In-Sb [59]. A recent high-resolution TEM study by Bourgeois et al. [60], however, argued that the major influence of Sn addition in Al-Cu alloys is to promote the nucleation of *θ'* with "magic" thicknesses (e.g. $3.5c_{\theta'}$ and $5.5c_{\theta'}$), corresponding to minima in volumetric and shear misfit strain. On the other hand, due to the limited experimental studies in recent years, the microalloying mechanisms by which Cd and In enhance the strength of Al-Cu alloys are less clear.

Based on the inspiring microalloying effects in age-hardenable Al-Cu alloys, it is of great interest to find a similar microalloying approach to enhance the precipitation of dispersoids in AA3xxx alloys. In this work, it is demonstrated that a minor addition of Cd (0.05 at.%) can dramatically change the nucleation behaviour of dispersoids and substantially enhance the precipitation of dispersoids and their dispersion hardening effect. To explore the superior strengthening effect induced by Cd addition, the microstructural evolution of dispersoids (including size, number density, morphology and spatial distribution) during the continuous heating until 600 °C was systematically investigated in comparison with a Cd-free 3003 alloy. APT has been applied to reveal the precipitation behaviour of Cd-rich nanoparticles and the nucleation behaviour of dispersoids in the low-temperature range.

2 Experimental

A DC-cast 3003 alloy extrusion billet with a dimension of 178 mm in diameter was used as the raw material and also as the reference material. After remelting at ~750 °C, a master alloy of

Al-5 wt.% Cd was added to the melt. When Cd was completely dissolved, the melt was kept for 30 min. In the end, the melt was cast into a copper mould to obtain a small ingot with a size of $100 \times 70 \times 30$ mm^3. The measured chemical compositions of both the 3003_0.2Cd alloy and the reference 3003 alloy are listed in Table 1. In comparison to the reference alloy, the contents of Mn, Fe and Si are slightly lower in the 3003_0.2Cd alloy, showing some loss of the alloying elements or dilution from the Al-Cd master alloy during remelting.

10 samples were cut from each as-cast ingot and subsequently heated up to 600 °C at a rate of 50 °C/h in an air circulation furnace. During the continuous heating between 150 and 600 °C, the samples were withdrawn and water quenched one by one at every 50 °C. Vickers hardness measurements were performed on samples after polishing with 1 μm surface finish using a load of 5 kg and a dwell time of 15 s. Each data point in the hardness curves was based on an average of at least 8 measurements. Electrical conductivity (EC) measurements were carried out on a planar, polished surface of the samples ($15 \times 15 \times 10$ mm^3) at room temperature (RT, 25 ± 1 °C) using a Foerster Sigmatest 2.069 instrument with a frequency of 60 kHz. The device was calibrated with two standard samples with given EC values (58.5 and 4.415 MS/m) before each testing to ensure the measurement accuracy. Flat rectangular tensile samples were machined based on ASTM standard with a gauge length of 25 mm. Ambient tensile testing was conducted on an MTS 810 tensile testing machine at an initial strain rate of 0.001 s^{-1}. An extensometer was used for the precise measurement of the strain. Three samples were tested for each condition and the average values were obtained.

A scanning electron microscope (FEI Quanta 650 FEG) was employed for the low-magnification observation of dispersoid distribution. Thin foils for transmission electron microscopy (TEM) study were prepared by a standard mechanical polishing and electropolishing procedure. Electropolishing was conducted using a solution of 1/3 HNO_3 in

methanol (maintained at ~ -25 °C) through a Struers TenuPol-5 twin-jet electropolisher operated at ~20 V. A JEOL 2100 operated at 200 kV was utilized for bright-field TEM imaging, selected area electron diffraction (SAED) and energy-dispersive X-ray spectroscopy (EDS) analyses. The number density of particles is determined by $N_V = \frac{N}{A(\bar{D}+t)}$ [33,34,38,61], where N is the number of particles within the TEM image, A is the area of the image, $\bar{D}$ is the average equivalent circular diameter of particles and t is the thickness of TEM foil for the local imaging area. For each sample, a series of TEM images (at least 8 areas) from the centre to the periphery of dendrite arms were taken and 200~2000 particles were analysed with the help of ImageJ software as well as manual measurements to obtain $\bar{D}$ and N. The local thickness (t) of TEM thin foil for each image was measured by electron energy loss spectroscopy (EELS). In addition, a JEOL 2100F operated at 200 kV was used to acquire high-angle annular dark-field scanning transmission electron microscopy (HAADF-STEM) images and the corresponding EDS data.

APT was used to characterize the early-stage precipitation of dispersoids. The needle-shaped APT samples were fabricated from small rods ($0.5 \times 0.5 \times 15$ mm^3) with a standard two-step electropolishing procedure. The first step was conducted with a solution of 30% perchloric acid in acetic acid at 20 V and the second step with a solution of 5% perchloric acid in 2-butoxyethanol at 20 V. APT characterization was carried out on a local electrode atom probe LEAP4000X SI under a high vacuum of 2×10^{-9} Pa, at a specimen temperature of 20 K, a UV laser pulsing energy of 40 pJ, a repetition rate of 250 kHz and a target evaporation rate of 0.5%. The detection efficiency of APT is ~55%, which is sufficient for the concentration measurements in this study. Atom probe data reconstruction and quantitative analyses were performed by using Cameca IVAS 3.6.12.

3 Results

3.1 Vickers hardness and electrical conductivity

The evolution of Vickers hardness and EC of the 3003 and 3003_0.2Cd alloys during continuous heating is presented in Figure 1. In the as-cast state, the 3003_0.2Cd alloy has a lower hardness but a higher EC value than the 3003 alloy. It is known that the solute Mn has an influence of decreasing the EC value of Al alloy [38], and Cd has the same effect but to a much lesser extent [62]. Therefore, the lower hardness but higher EC value of the 3003_0.2Cd alloy is most likely to be correlated with a lower content of Mn in solid solution. During heating, the hardness of the 3003 alloy starts to increase after it is heated to 300 °C and reaches a maximum value at 450 °C. The hardness evolution is consistent with the EC evolution of the alloy, as shown in Figure 1(b). The increases of EC at 300-450 °C suggests the decomposition of SSSS and the precipitation of dispersoids, while the decrease of EC at 450-600 °C is an indication of the dissolution of dispersoids and thus an increase of Mn concentration in solid solution [38,63]. For the 3003_0.2Cd alloy, although its EC evolution looks similar to that of the 3003 alloy, this alloy has two hardness peaks at 200°C and 450°C, respectively. The peak hardness at 450 °C (49.2 ± 0.5 HV) is much higher than that of the base alloy (44.3 ± 0.6 HV), indicating that the Cd addition has substantially increased the dispersion strengthening by dispersoids in the alloy. The unexpected peak hardness at 200 °C is 46.5 ± 0.6 HV. At this peak-hardness temperature, however, little change of EC is detected (Figure 1(b)), suggesting that an additional strengthening phase other than α-Al(Mn,Fe)Si dispersoid is formed. Moreover, in contrast to an almost constant EC value of the 3003 alloy from RT to 300 °C, an increase of EC becomes evident at 300 °C in the 3003_0.2Cd alloy (Figure 1(b)), which indicates an earlier dispersoid precipitation than the 3003 alloy.

3.2 Precipitation of α-Al(Mn,Fe)Si dispersoids

The representative SEM micrographs of the two experimental alloys as-heated to 450 °C (the peak-hardness temperature) are shown in Figure 2. Fine dispersoids are observed in both alloys, but the density of the dispersoids in the 3003_0.2Cd alloy is significantly higher than that in the 3003 alloy. Furthermore, the distribution of dispersoids in the 3003 alloy shows a network like character (Figure 2(a)), which is likely due to the preferential nucleation of the dispersoids along dislocations [38]. In contrast, the distribution of dispersoids in the 3003_0.2Cd alloy is much more homogeneous; only in the regions close to the large constituent particles (with bright contrast) at dendrite arm periphery, the number density of dispersoids is lower (Figure 2(b)).

TEM micrographs of the 3003_0.2Cd alloy during heating in the range of 350-600 °C are shown in Figure 3. In the sample as-heated to 350 °C, as shown in Figure 3 (a), a high density of nano-sized particles with a dark grey contrast have formed in the Al matrix. A few relatively coarse nanoparticles with a dark contrast (pointed by white arrows) can also be observed. A careful examination reveals that most of the dark nanoparticles are associated with dark grey nanoparticles. EDS analyses show that the dark grey nanoparticles are most likely to be α-Al(Mn,Fe)Si dispersoids (see inset 1 in Figure3(a)), while the dark nanoparticles are enriched with Cd (see inset 2 in Figure 3(a)). An increase of temperature to 400 °C leads to an evident increase of the dispersoid size, but no evident decrease in the number density is observed (Figure 3(b)). In the sample as-heated to 450 °C, although some relatively coarse dispersoids can be seen, most of the dispersoids are still in the nano-sized range and the density is also high (Figure 3(c)). The SAED pattern of multiple dispersoids along [111] zone axis of the α-Al (inset in Figure 3(c)) shows a six-fold pattern of reflections from α-dispersoids which is the same as that shown in Ref. [25], confirming that these α-Al(Mn,Fe)Si dispersoids have the same preferential OR with the Al matrix.

At 500 °C, a further coarsening of dispersoids is evident (Figure 3(d)). It should be noted that the majority of dispersoids have a roughly cubic shape up to 500 °C and only a small fraction of them are in thin platelet or rod morphology (Figure 3(a)-(d)). This is different from the dispersoids in the 3003 alloy as-heated to 500 °C, where a large fraction of dispersoids have a thick platelet morphology [38]. Dispersoids in the 3003_0.2Cd alloy as-heated to 550 and 600 °C become even coarser and the number density continuously decreases (Figure 3(e) and (f)). Some dispersoids exhibit a thick platelet morphology. Interestingly, nanoparticles with a dark contrast (labelled by white arrows in Figure 3(e) and (f)) are observed to be attached to the coarse α-dispersoids.

HAADF-STEM and EDS analyses were employed to identify the dark nanoparticles attached to dispersoids as seen in Figure 3. In the HAADF-STEM image (Figure 4(a)), the nanoparticles show a bright contrast while the coarse dispersoids show a dark grey contrast. EDS line scanning across one dispersoid with a nanoparticle (Figure 4(b)) indicates that the dark grey dispersoid is enriched with Mn, Si and Fe, while the bright nanoparticle is Cd-rich in nature.

Figure 5 summarizes the measured equivalent diameter, number density and size distribution of dispersoids in the 3003_0.2Cd alloy as-heated to different temperatures. The statistical data of the 3003 alloy subjected to the same heat treatment [38] is also included for comparison. It is revealed that between 350 and 500 °C, the size of dispersoids in the 3003_0.2Cd alloy is smaller while the number density is much higher than that in the 3003 alloy at the same temperature (Figure 5 (a) and (b)). However, the difference in size between the two alloys is less evident at the nucleation/growing stage (350-400 °C), while the difference in number density is less evident after heating to a higher temperature (≥ 500 °C). At the peak-hardness temperature of 450 °C, the number density of dispersoids in the 3003_0.2Cd alloy (~2200 μm^{-3}) is almost doubled as that of the 3003 alloy (~1200 μm^{-3}). Although the dispersoids seem to be coarsening during heating from 350 to 450 °C according to the statistical data, the maximum

EC value and hardness are achieved at 450 °C. This should be attributed to the increase in the total volume fraction of dispersoids due to the size increase. On the other hand, the dispersoids at 550-600 °C show almost the same size and density as that of the 3003 alloy at the same temperature (Figure 5). It indicates that at higher temperatures, dispersoids in the 3003_0.2Cd alloy experienced a fast dissolution as those in the 3003 alloy due to the solubility increase of Mn in Al [38]. According to the microstructural analyses shown in Figure 2, 3 and 5, the addition of Cd is effective in obtaining finer, denser and more homogeneously distributed dispersoids at temperatures between 350 and 500 °C.

3.3 Early-stage precipitation of Cd-rich nanoparticles and dispersoids

Figure 6(a)-(d) show a series of TEM micrographs of nanoparticles precipitated in the 3003_0.2Cd alloy as-heated to temperatures between 200 and 350 °C. At 200 °C, well-dispersed ultrafine nanoparticles with an average diameter of 1.5 nm are found in the Al matrix (Figure 6(a)). After the alloy is heated to 250 °C, a slight increase in the size of nanoparticles can be observed (Figure 6(b)). TEM-EDS analyses reveal that these nanoparticles are enriched with Cd (see inset). When the alloy is further heated to 300 °C, both the nano-sized dark grey particles (pointed by red arrows in Figure 6(c)) and "composite" particles (with a dark component and a dark grey component, as indicated by white arrows) can be observed. HAADF-STEM images of two "composite" particles and the corresponding EDS line scan profiles across the particles are shown in Figure 7. It reveals that the dark grey components of the "composite" particles in the bright-field image are enriched with Mn, Si and Fe, while the dark components are enriched with Cd. It implies that the precipitation of α-Al(Mn,Fe)Si dispersoids is correlated with the Cd-rich nanoparticles. At 350 °C, more α-Al(Mn,Fe)Si dispersoids with an increase in size can be found (Figure 6(d)), while the "composite" nanoparticles are less frequently observed.

Figure 8 presents the evolution of average equivalent diameter and number density of Cd-rich nanoparticles and α-Al(Mn,Fe)Si dispersoids in the 3003_0.2Cd alloy as-heated to 200-350 °C. With the increase of temperature, the average size of Cd-rich nanoparticles increases while the number density decreases, suggesting that the Cd-rich nanoparticles experience a coarsening and/or dissolution process between 200 and 350 °C. It is interesting to see that when the temperature increases from 300 to 350 °C, the number density of Cd-rich nanoparticles significantly reduces from 1500 μm^{-3} to 100 μm^{-3} while the number density of dispersoids is almost doubled from 1300 μm^{-3} to 2500 μm^{-3} (Figure 8). In combination with the TEM observations shown in Figure 6, it is suggested that during heating from 300 to 350 °C, many Cd-rich nanoparticles of the "composite" particles are coarsened and/or dissolved while the dispersoids of the "composite" particles remain and continue to grow.

To explore the crystal structure of the Cd-rich nanoparticles, SAED analyses were conducted. Two different types of Cd-rich nanoparticles were identified. Figure 9(a) and (d) show bright-field TEM images of two coarse Cd-rich nanoparticles with a diameter of 40-60 nm in the 3003_0.2Cd alloy as-heated to 250-300 °C. Figure 9(b) and (e) show their corresponding SAED patterns, which were taken along $[\bar{1}\bar{1}0]_m$ and $[\bar{1}11]_m$, respectively. The coarse Cd-rich nanoparticles are determined to have a hexagonal close-packed (hcp) crystal structure as the equilibrium Cd phase (*P*6$_3$*/mmc*, a = 0.298 nm, c = 0.562 nm). The orientation relationship between the hcp Cd-rich particles and Al matrix is determined to be $(11\bar{2}0)_p \parallel (220)_m, [0001]_p \parallel [\bar{1}11]_m$, which is consistent with the simulated diffraction patterns shown in Figure 9(c) and (f). On the other hand, most of the Cd-rich nanoparticles observed in this study show a size less than 16 nm (Figure 6, 8 and 10(a)), the corresponding SAED patterns reveal no extra diffraction spot except for the spots of α-Al (Figure 10(b) and (c)), indicating that the Cd-rich nanoparticles might have a metastable form with the same crystal structure and a similar lattice constant as the Al matrix. However, this needs yet to be further investigated.

3.4 Formation of Mn-rich clusters

APT was employed to further investigate the role of Cd-rich nanoparticles played in the early stage of α-Al(Mn,Fe)Si dispersoid precipitation. Figure 11 shows the APT results of the 3003_0.2Cd alloy as-heated to 250 °C, where the Cd atoms are displayed in green, Mn in yellow and Si in grey. Since the signals of Fe^{2+} ions in the mass spectrum is mostly overlapping with the main peak of Al^{+1} ions, Fe was not clearly identified. Nano-sized Cd-rich particles are evidenced in the Cd atom map as shown in Figure 11(a). Although the enrichments of Mn and Si in the Cd-rich particles are hard to be resolved by visual examination of the total Mn and Si atom maps, their enrichments are clearly resolved in a zoomed view of a Cd-rich particle (in a blue box in Figure 11(b)) in a thin slice as shown in Fig. 11(c). A proximity histogram (proxigram) of the Cd-rich particle defined by an isoconcentration surfaces at 4.6 at.% Cd (Figure 11(c)) reveals that the maximum Cd concentration of the particle is about 19.50 at.% measured from its central region (Figure 11(c)). This implies that the Cd-rich nanoparticles are Al-Cd precipitates rather than the stable pure Cd phase. It is striking to see that the concentration of Mn within the Cd-rich region (2.34 ± 0.36 at.%) is much higher than that in the surrounding Al matrix (0.37 ± 0.05 at.%). An almost doubled Si concentration is detected at the periphery of Cd-rich nanoparticles (0.40 ± 0.10 at.%) when compared to the Al matrix (0.20 ± 0.04 at.%). However, the peak of Mn concentration slightly deviates from the centre of Cd-rich region, which shows a “core-shell” structure. It implies that the Cd-rich nanoparticles may form first, and Mn and Si atoms diffuse and partition to the Cd-rich nanoparticles later. Figure 11(d) presents the proxigram of a smaller Cd-rich nanoparticle with a radius of about 1.5 nm (in an orange dashed box in Figure11(b)). The concentration peaks of Mn and Si also deviate from the centre of the nanoparticle, confirming the “core-shell” structure of Cd-rich nanoparticles. In comparison to the larger particle in Figure 11(c), the concentrations of Mn,

Si and Cd in this particle are smaller, which implies that the enrichments of these elements increase with the size of Cd-rich nanoparticles.

3.5 Tensile results and dispersoid strengthening

The engineering stress-strain curves of both the 3003 and 3003_0.2Cd alloys as-heated to 450 °C are presented in Figure 12. The yield strength (YS), ultimate tensile strength (UTS) as well as total elongation (TE) are listed in Table 2. As can be seen, the YS of the 3003_0.2Cd alloy is 17 MPa higher than that of the 3003 alloy, which is corresponding to an improvement of 25%. This is in a good agreement with the observed higher density and finer size of dispersoids in the 3003_0.2Cd alloy.

To quantitatively address the dispersion strengthening effect, the measured yield strength of the 3003_0.2Cd alloy as-heated to 450 °C was compared with the 3003_0.2Cd alloy homogenized at 600 °C for 24 h, where all the dispersoids have dissolved. The almost equal EC values of the two samples indicates a similar level of Mn concentrations, and consequently, a similar solid solution strengthening. It can be calculated that the dispersion strengthening due to dispersoid precipitation in the 3003_0.2Cd alloy as-heated to 450 °C is 37 MPa.

By using the Orowan looping mechanism, the increase of yield strength contributed by dispersoids, $\Delta\sigma_p$, can be also theoretically assessed [64]:

$$\Delta\sigma_p = \frac{0.84MGb}{2\pi(1-v)^{1/2}\lambda} ln\frac{r}{b} \quad (1)$$

where M is the Taylor factor, G is the shear modulus of the matrix, b is the magnitude of the Burgers vector, v is the Poisson ratio, r is the equivalent radius of dispersoids and λ is the interparticle spacing which can be determined by:

$$\lambda = r \cdot (\frac{2\pi}{3f})^{1/2} \quad (2)$$

where *f* is the volume fraction of dispersoids. Based on the statistical analyses of dispersoids at 450 °C, the equivalent radius is 11.1 nm, the dispersoid free zone is measured as 15% and the corresponding volume fraction is calculated to be 0.52% using the method described in Ref. [38] assuming a cubic shape of all dispersoids. Taking $M = 2$, $G = 27.4$ GPa, $|b| = 0.286\ nm$, $\upsilon = 0.33$ [19], the calculated $\Delta\sigma_p$ is 41 MPa, which is slightly higher than the measured increment of the yield strength, 37 MPa. This discrepancy is partially associated with a slightly lower solid solution strengthening of the sample as-heated to 450 °C than the homogenized sample (600 °C, 24 h), as indicated by the EC values in Table 2. Another reason for the discrepancy may be related to the simplification of all dispersoids as a cubic shape when calculating the volume fraction, while TEM observations reveal that many dispersoids deviate from the perfect cubic shape and a small fraction of dispersoids show a rod- or platelet-shaped morphology (Figure 3(c)). The shape effect on the measured volume fraction of dispersoids based on 2D TEM images has been discussed in detail in Ref. [38].

4 Discussion

4.1 Precipitation of Cd-rich nanoparticles

It is interesting to see that a high number density of Cd-rich nanoparticles (more than 10^4 μm^{-3}) formed at 200-250 °C prior to α-Al(Mn,Fe)Si dispersoid precipitation in the 3003_0.2Cd alloy (Figure 6). A phase diagram calculation was carried out by using Thermo-Calc software based on the thermodynamic database TCAL4 [65] to show the temperature-dependent Cd solubility in a 3003 alloy with the chemical composition of Al-1.1Mn-0.5Fe-0.18Si (Figure 13). It shows that the solubility of Cd in the Al matrix (highlighted in red) reaches a maximum of 0.52 wt.% at 635 °C and decreases gradually with decreasing temperature. At temperatures

below 300 °C, Cd has a very limited solubility (≤ 0.01 wt.%). Due to the fast cooling during solidification of the as-cast 3003_0.2Cd alloy, most of the Cd atoms are supposed to be in the solid solution and the Al matrix is supersaturated with Cd. Therefore, during the following heating process until 300 °C, there is a strong driving force for the decomposition of the SSSS, which leads to the precipitation of Cd-rich nanoparticles. On the other hand, although Mn is also supersaturated in the Al matrix below 300 °C, the diffusivity of Mn is much lower than that of Cd. For instance, the diffusion coefficients of the two alloying elements at 200 °C are 6.1×10^{-22} cm^2s^{-1} and 2.0×10^{-14} cm^2s^{-1} ,respectively [66–68]. It means that the precipitation of Cd-rich nanoparticles will be much faster than that of Mn-containing dispersoids during heating at low temperatures. This is the reason why Cd-rich nanoparticles could precipitate at 200-250 °C prior to α-Al(Mn,Fe)Si dispersoids during the continuous heating.

According to the previous studies on Cd-containing Al alloys, the decomposition of Cd-supersaturated solid solution generally leads to the formation of equilibrium hcp Cd phase or intermediate hcp Cd' phase with reduced lattice parameters [40,43]. Here, it is surprising that a high density of ultrafine nano-sized metastable Al-Cd precipitates were formed in the 3003_0.2Cd alloy during heating at 150-250 °C. APT results suggest these Al-Cd precipitates have an approximate constitution of Al_3Cd or Al_4Cd. SAED analyses indicate that the Al-Cd precipitate has a crystal structure different from the hcp Cd or Cd' phases. To the authors' knowledge, such a metastable Al-Cd phase has never been reported before. A further research work is yet needed for the determination of its exact crystal structure. In addition, the hardness results in this study reveal that these ultrafine Al-Cd precipitates formed during heating between 150 and 250 °C have a significant precipitation hardening effect (Figure 1(a)), which is also worthy of further investigation.

It seems that the crystal structure of Al-Cd phase is sensitive to the particle size and temperature. At the temperatures between 250 and 300 °C, some of the Cd-rich nanoparticles have become rather coarse, with a diameter of 40-60 nm (Figure 9(a) and (d)). With such a size, the metastable Al-Cd precipitates have transformed to the stable Cd phase with a hcp crystal structure (Figure 9(b) and (e)).

4.2 Mechanism of dispersoid precipitation on Cd-rich nanoparticles

In AA 3xxx alloy, the precipitation of α-Al(Mn,Fe)Si dispersoids is usually very sluggish during continuous heating due to the low diffusion coefficient of Mn. In most cases, the earliest dispersoid precipitation was observed at 300~350 °C depending on the heating rate and alloy composition, and the preferential nucleation sites have been revealed to be dislocations [38]. However, the density of dislocations is very limited in as-cast ingots, which therefore results in a rather low number density of dispersoids [33,38]. In this work, we have shown that with a minor addition of Cd (0.05 at.%), the precipitation of dispersoids and consequently their dispersion strengthening are dramatically improved. TEM and APT investigations reveal that this improvement is related to a new nucleation mechanism of the dispersoids induced by Cd addition.

The TEM images in Figure 6 and HAADF-STEM images in Figure 7 show that, in the early stage of precipitation (~ 300 °C), a large fraction of the dispersoids in the 3003_0.2Cd alloy are associated with Al-Cd precipitates which precipitate at lower temperatures (as early as 150 °C). According to the TEM and APT examinations (Figure 6(c) and 11), there is no precipitation of α-Al(Mn,Fe)Si dispersoids in the 3003_0.2Cd alloy as-heated to 250 °C. Instead, a high number density of Al-Cd precipitates (~10^4 μm^{-3}) are detected (Figure 6(b) and 8). It suggests that the metastable Al-Cd precipitates may have acted as nucleation sites for dispersoids.

The most striking result revealed by APT is the enrichment of Mn and Si atoms in/around the Al-Cd precipitates at 250°C (Figure 11). The "core-shell" structure (Figure 11(c)) indicates that the supersaturated Mn (maybe also Fe) and Si atoms in the Al matrix prefer to diffuse and partition to Cd-rich atomic clusters. It should be noted that, although attached together, the Al-Cd precipitates and Mn,Si-rich clusters have grown independently, as illustrated in Figure 6. With the temperature increasing from 200 to 350 °C, the average size of Al-Cd precipitates increases while the number density drops sharply (Figure 8). On the other hand, since the diffusion of Mn and Fe in Al are very slow compared to that of Cd, the coarsening of the Mn,Si-rich clusters is rather sluggish. Those Mn,Si-rich clusters previously attached to the Al-Cd precipitates may survive in the matrix when those smaller Al-Cd precipitates dissolve due to coarsening and solubility increase of Cd. With increasing temperature, the partitioning of Mn and Si atoms to these clusters will be accelerated due to the increased diffusion coefficients of the elements. Once the size of the cluster reaches the critical nucleation radius while the chemical composition of the cluster reaches the critical concentration at a higher temperature, α-Al(Mn,Fe)Si dispersoids will form. In the 3003_0.2Cd alloy as-heated to 300 °C, the unattached α-Al(Mn,Fe)Si dispersoids (indicated by red arrows in Figure 6(c)) have a number density of ~1300 μm^{-3}, which is substantially higher than that of the dispersoids in the Cd-free 3003 alloy subjected to the same heat treatment (barely visible with $N_v < 500\ \mu m^{-3}$) [38]. Most of the unattached dispersoids in the 3003_0.2Cd alloy as-heated to 300 °C are supposed to be the product of the further growth of those survived Mn,Si-rich clusters.

Such a nucleation behaviour of α-dispersoids has some similarities with the heterogeneous nucleation of *θ'* in Sn-containing Al-Cu alloys reported by Homma et al. [46]. In their work, the clustering of Cu atoms with Sn atoms was observed in the early stage of ageing at 200 °C, followed by the *θ'* precipitation at *β*-Sn precipitate. The difference is that in the 3003_0.2Cd alloy, even after the foreign substrate Al-Cd precipitates have dissolved into the Al matrix, α-

dispersoids can precipitate from the remaining Mn,Si-rich clusters. Most importantly, the TEM and SEM observations demonstrate that this new nucleation approach of dispersoids assisted by Al-Cd precipitates is much more efficient than the conventional nucleation on dislocations: the earlier-formed Al-Cd precipitates with Mn,Si-rich clusters accelerate the precipitation of dispersoids during continuous heating, and their high number density also makes the homogeneous distribution of dispersoids possible.

It has to be noted that Cd is a poisonous element, so it is difficult to use Cd in commercial Al alloys. However, the highlight of this work is that we have shown an effective approach to promote the nucleation of dispersoids and therefore the dispersion hardening effect of aluminium alloy. More interestingly, it has been revealed that the effect of Cd addition on enhancing the nucleation of dispersoids is similar to its effect on enhancing the nucleation of age-hardening precipitates. Therefore, other alloying additions which have shown similar effects as Cd in age-hardening precipitates (e.g. In or Sn) are worth investigating in terms of enhancing the dispersoid precipitation. It also needs to mention that a further improved dispersion hardening effect can be expected via an optimization of the heat treatment. For example, a higher yield strength by annealing at 375 °C for 24 h (86.6 MPa) than that by as-heated to 450 °C (73.1 MPa) has been reported in a 3xxx alloy [33].

5 Conclusions

In this work, we have demonstrated an effective strategy to enhance the dispersion hardening effect of α-Al(Mn,Fe)Si dispersoids in aluminium alloys with a small addition of impurity element Cd (0.05 at%). The precipitation behaviour of α-dispersoids as well as their dispersion hardening effect in the 3003 alloys with/without Cd addition during continuous heating up to 600 °C were systematically investigated by employing hardness, EC, tensile test, SEM, TEM, and APT. The following conclusions can be drawn from the experimental results:

1. An addition of 0.05 at.% Cd can substantially enhance the nucleation and therefore to achieve a higher number density of nano-sized α-Al(Mn,Fe)Si dispersoids in the temperature range of 350-500 °C during continuous heating. At the peak-hardness temperature of 450 °C, the number density of α-dispersoids in the Cd-containing alloy is about twice as that of the 3003 base alloy. Accordingly, an increase of YS by 25% is achieved with Cd addition. A comparison to the 3003 alloy as-homogenized at 600°C for 24h shows that the precipitation of α-Al(Mn,Fe)Si dispersoids in the Cd-containing alloy as-heated to 450 °C can provide an increase of yield strength by 37 MPa.
2. The addition of Cd changes the nucleation behaviour of α-Al(Mn,Fe)Si dispersoids from the heterogeneous nucleation on dislocations to a more homogeneous nucleation on Mn,Si-rich clusters forming at Cd-rich nanoparticles. During continuous heating, a high number density ($\geq 10^{22}$ m^{-3}) of Cd-rich nanoparticles with a diameter of ~2 nm precipitate at 200-250 °C. An APT study shows that these ultrafine Cd-rich nanoparticles can attract Mn and Si atoms to form Mn,Si-rich clusters in/around them, which act as the precursors of α-Al(Mn,Fe)Si dispersoids formed at higher temperatures, ~300 °C.
3. The Cd-rich nanoparticles experienced a phase transformation during heating. The majority of ultrafine Cd-rich nanoparticles formed at 150-250 °C have a metastable form with an Al_3Cd or Al_4Cd constitution. These Al-Cd precipitates show a significant precipitation hardening effect during heating, with a peak hardness at 200 °C. When growing into a larger size of 40-60 nm at higher temperatures, Cd-rich nanoparticles transform to the equilibrium hcp Cd phase, which has an OR of $(11\bar{2}0)_p \parallel (220)_m, [0001]_p \parallel [\bar{1}11]_m$ with the Al matrix.

Acknowledgements

The Norwegian Centre of Transmission Electron Microscopy (NORTEM) at NTNU, where the TEM work was carried out, is gratefully acknowledged. FQ would like to thank the help from Di Wan for the SEM operation.

References

[1] S.B. Wang, J.H. Chen, M.J. Yin, Z.R. Liu, D.W. Yuan, J.Z. Liu, et al., Double-atomic-wall-based dynamic precipitates of the early-stage S-phase in AlCuMg alloys, Acta Materialia. 60 (2012) 6573–6580. doi:10.1016/j.actamat.2012.08.023.

[2] R. Holmestad, R. Bjørge, F.J.H. Ehlers, M. Torsæter, C.D. Marioara, S.J. Andersen, et al., Characterization and structure of precipitates in 6xxx Aluminium Alloys, Journal of Physics: Conference Series. 371 (2012) 012082. doi:10.1088/1742-6596/371/1/012082.

[3] C.B. Fuller, D.N. Seidman, D.C. Dunand, Creep properties of coarse-grained Al(Sc) alloys at 300°C, Scripta Materialia. 40 (1999) 691–696. doi:10.1016/S1359-6462(98)00468-0.

[4] E. Marquis, D.. Seidman, Nanoscale structural evolution of Al3Sc precipitates in Al(Sc) alloys, Acta Materialia. 49 (2001) 1909–1919. doi:10.1016/S1359-6454(01)00116-1.

[5] S.P. Wen, K.Y. Gao, Y. Li, H. Huang, Z.R. Nie, Synergetic effect of Er and Zr on the precipitation hardening of Al–Er–Zr alloy, Scripta Materialia. 65 (2011) 592–595. doi:10.1016/j.scriptamat.2011.06.033.

[6] S.P. Wen, K.Y. Gao, H. Huang, W. Wang, Z.R. Nie, Precipitation evolution in Al–Er–Zr alloys during aging at elevated temperature, Journal of Alloys and Compounds. 574 (2013) 92–97. doi:10.1016/j.jallcom.2013.03.237.

[7] H. Li, J. Bin, J. Liu, Z. Gao, X. Lu, Precipitation evolution and coarsening resistance at 400 °C of Al microalloyed with Zr and Er, Scripta Materialia. 67 (2012) 73–76. doi:http://dx.doi.org/10.1016/j.scriptamat.2012.03.026.

[8] H. Li, Z. Gao, H. Yin, H. Jiang, X. Su, J. Bin, Effects of Er and Zr additions on precipitation and recrystallization of pure aluminum, Scripta Materialia. 68 (2013) 59–62. doi:10.1016/j.scriptamat.2012.09.026.

[9] C.B. Fuller, D.N. Seidman, D.C. Dunand, Mechanical properties of Al(Sc,Zr) alloys at ambient and elevated temperatures, Acta Materialia. 51 (2003) 4803–4814. doi:10.1016/S1359-6454(03)00320-3.

[10] C. Fuller, J. Murray, D. Seidman, Temporal evolution of the nanostructure of Al(Sc,Zr) alloys: Part I – Chemical compositions of Al(ScZr) precipitates, Acta Materialia. 53 (2005) 5401–5413. doi:10.1016/j.actamat.2005.08.016.

[11] C. Fuller, D. Seidman, Temporal evolution of the nanostructure of Al(Sc,Zr) alloys: Part II-coarsening of Al(ScZr) precipitates, Acta Materialia. 53 (2005) 5415–5428. doi:10.1016/j.actamat.2005.08.015.

[12] A. Tolley, V. Radmilovic, U. Dahmen, Segregation in Al3(Sc,Zr) precipitates in Al–Sc–Zr alloys, Scripta Materialia. 52 (2005) 621–625. doi:10.1016/j.scriptamat.2004.11.021.

[13] E. Clouet, L. Laé, T. Epicier, W. Lefebvre, M. Nastar, A. Deschamps, Complex precipitation pathways in multicomponent alloys., Nature Materials. 5 (2006) 482–8. doi:10.1038/nmat1652.

[14] A. Deschamps, L. Lae, P. Guyot, In situ small-angle scattering study of the precipitation kinetics in an Al–Zr–Sc alloy, Acta Materialia. 55 (2007) 2775–2783. doi:10.1016/j.actamat.2006.12.015.

[15] K.E. Knipling, R.A. Karnesky, C.P. Lee, D.C. Dunand, D.N. Seidman, Precipitation evolution in Al–0.1Sc, Al–0.1Zr and Al–0.1Sc–0.1Zr (at.%) alloys during isochronal aging, Acta Materialia. 58 (2010) 5184–5195. doi:10.1016/j.actamat.2010.05.054.

[16] K.E. Knipling, D.N. Seidman, D.C. Dunand, Ambient- and high-temperature mechanical properties of isochronally aged Al–0.06Sc, Al–0.06Zr and Al–0.06Sc–0.06Zr (at.%) alloys, Acta Materialia. 59 (2011) 943–954. doi:10.1016/j.actamat.2010.10.017.

[17] K. Liu, X.-G. Chen, Development of Al–Mn–Mg 3004 alloy for applications at elevated temperature via dispersoid strengthening, Materials & Design. 84 (2015) 340–350. doi:10.1016/j.matdes.2015.06.140.

[18] K. Liu, X.-G. Chen, Influence of heat treatment and its sequence on elevated-temperature properties of Al-Mn-Mg 3004 alloy, Materials Science and Engineering: A. 697 (2017) 141–148. doi:10.1016/j.msea.2017.05.027.

[19] Y.J. Li, A.M.F. Muggerud, A. Olsen, T. Furu, Precipitation of partially coherent α-Al(Mn,Fe)Si dispersoids and their strengthening effect in AA 3003 alloy, Acta Materialia. 60 (2012) 1004–1014. doi:10.1016/j.actamat.2011.11.003.

[20] Y.J. Li, W.Z. Zhang, K. Marthinsen, Precipitation crystallography of plate-shaped Al6(Mn,Fe) dispersoids in AA5182 alloy, Acta Materialia. 60 (2012) 5963–5974. doi:10.1016/j.actamat.2012.06.022.

[21] S. Esmaeili, D. Vaumousse, M.W. Zandbergen, W.J. Poole, A. Cerezo, D.J. Lloyd, A study on the early-stage decomposition in the Al–Mg–Si–Cu alloy AA6111 by electrical resistivity and three-dimensional atom probe, Philosophical Magazine. 87 (2007) 3797–3816. doi:10.1080/14786430701408312.

[22] Y. Li, L. Arnberg, Evolution of eutectic intermetallic particles in DC-cast AA3003 alloy during heating and homogenization, Materials Science and Engineering: A. 347 (2003) 130–135. doi:10.1016/S0921-5093(02)00555-5.

[23] Y. Li, L. Arnberg, Precipitation of Dispersoids in DC-Cast AA3103 Alloy during Heat Treatment BT - Essential Readings in Light Metals: Volume 3 Cast Shop for Aluminum Production, in: J.F. Grandfield, D.G. Eskin (Eds.), Essential Readings in Light Metals, Springer International Publishing, Cham, 2016: pp. 1021–1027. doi:10.1007/978-3-319-48228-6_129.

[24] Y.J. Li, L. Arnberg, Precipitation of Dispersoids in DC-Cast 3003 Alloy, Materials Science Forum. 396–402 (2002) 875–880. doi:10.4028/www.scientific.net/MSF.396-402.875.

[25] M. Cooper, K. Robinson, The crystal structure of the ternary alloy α(AlMnSi), Acta Crystallographica. 20 (1966) 614–617. doi:10.1107/S0365110X6600149X.

[26] M. Cooper, The crystal structure of the ternary alloy α(AlFeSi), Acta Crystallographica. 23 (1967) 1106–1107. doi:10.1107/S0365110X67004372.

[27] A.M.F. Muggerud, J.C. Walmsley, R. Holmestad, Y. Li, Combining HAADF STEM tomography and electron diffraction for studies of α-Al(Fe,Mn)Si dispersoids in 3xxx aluminium alloys, Philosophical Magazine. 95 (2015) 744–758. doi:10.1080/14786435.2015.1006294.

[28] E. Nes, The effect of a fine particle dispersion on heterogeneous recrystallization, Acta Metallurgica. 24 (1976) 391–398. doi:10.1016/0001-6160(76)90059-6.

[29] F.J. Humphreys, The nucleation of recrystallization at second phase particles in deformed aluminium, Acta Metallurgica. 25 (1977) 1323–1344. doi:10.1016/0001-6160(77)90109-2.

[30] G. Hausch, P. Furrer, H. Warlimont, Recrystallization and precipitation in al-Mn-Si alloys, Z Metallkd. 69 (1978) 174–181.

[31] Y. Kwag, J.G. Morris, The effect of structure on the mechanical behavior and stretch formability of constitutionally dynamic 3000 series aluminum alloys, Materials Science and Engineering. 77 (1986) 59–74. doi:10.1016/0025-5416(86)90354-X.

[32] W.B. Hutchinson, A. Oscarsson, Å. Karlsson, Control of microstructure and earing behaviour in aluminium alloy AA 3004 hot bands, Materials Science and Technology. 5 (1989) 1118–1127. doi:10.1179/mst.1989.5.11.1118.

[33] A.M.F. Muggerud, E.A. Mørtsell, Y. Li, R. Holmestad, Dispersoid strengthening in AA3xxx alloys with varying Mn and Si content during annealing at low temperatures, Materials Science and Engineering: A. 567 (2013) 21–28. doi:10.1016/j.msea.2013.01.004.

[34] K. Liu, H. Ma, X.-G. Chen, Enhanced elevated-temperature properties via Mo addition in Al-Mn-Mg 3004 alloy, Journal of Alloys and Compounds. 694 (2017) 354–365. doi:10.1016/j.jallcom.2016.10.005.

[35] K. Liu, X.-G. Chen, Evolution of Intermetallics, Dispersoids, and Elevated Temperature Properties at Various Fe Contents in Al-Mn-Mg 3004 Alloys, Metallurgical and Materials Transactions B. 47 (2016) 3291–3300. doi:10.1007/s11663-015-0564-y.

[36] H. Hirasawa, Precipitation process of Al-Mn and Al-Cr supersaturated solid solution in presence of age hardening phases, Scripta Metallurgica. 9 (1975) 955–958. doi:https://doi.org/10.1016/0036-9748(75)90551-7.

[37] L. Lodgaard, N. Ryum, Precipitation of dispersoids containing Mn and/or Cr in Al–Mg–Si alloys, Materials Science and Engineering: A. 283 (2000) 144–152. doi:10.1016/S0921-5093(00)00734-6.

[38] Y.J. Li, L. Arnberg, Quantitative study on the precipitation behavior of dispersoids in DC-cast AA3003 alloy during heating and homogenization, Acta Materialia. 51 (2003) 3415–3428. doi:10.1016/S1359-6454(03)00160-5.

[39] H.K. Hardy, The ageing characteristics of ternary aluminium-copper alloys with cadmium, indium, or tin, Journal of the Institute of Metals. 80 (1951) 483.

[40] J.M. Silcock, T.J. Heal, H.K. Hardy, Intermediate precipitates in aged binary alloys of aluminium with cadmium, indium and tin, Journal of the Institute of Metals. 84 (1955) 23.

[41] H.K. Hardy, Aluminium-copper-cadmium sheet alloys, Journal of the Institute of Metals. 83 (1954) 337.

[42] B.T. Sofyan, K. Raviprasad, S.P. Ringer, Effects of microalloying with Cd and Ag on the precipitation process of Al–4Cu–0.3Mg (wt%) alloy at 200°C, Micron. 32 (2001) 851–856. doi:10.1016/S0968-4328(00)00093-7.

[43] J.M. Silcock, The structural ageing characteristics of ternary aluminium-copper alloys wih cadimium, indium, or tin, Journal of the Institute of Metals. 84 (1955) 23.

[44] L. Bourgeois, J.F. Nie, B.C. Muddle, Assisted nucleation of θ′ phase in Al–Cu–Sn: the modified crystallography of tin precipitates, Philosophical Magazine. 85 (2005) 3487–3509. doi:10.1080/14786430500228473.

[45] S.P. Ringer, K. Hono, T. Sakurai, The effect of trace additions of sn on precipitation in Al-Cu alloys: An atom probe field ion microscopy study, Metallurgical and Materials Transactions A. 26 (1995) 2207–2217. doi:10.1007/BF02671236.

[46] T. Homma, M.P. Moody, D.W. Saxey, S.P. Ringer, Effect of Sn Addition in Preprecipitation Stage in Al-Cu Alloys: A Correlative Transmission Electron Microscopy and Atom Probe Tomography Study, Metallurgical and Materials Transactions A. 43 (2012) 2192–2202. doi:10.1007/s11661-012-1111-y.

[47] C.D. Marioara, S.J. Andersen, T.N. Stene, H. Hasting, J. Walmsley, A.T.J. Van Helvoort, et al., The effect of Cu on precipitation in Al–Mg–Si alloys, Philosophical Magazine. 87 (2007) 3385–3413. doi:10.1080/14786430701287377.

[48] M.W. Zandbergen, A. Cerezo, G.D.W. Smith, Study of precipitation in Al–Mg–Si Alloys by atom probe tomography II. Influence of Cu additions, Acta Materialia. 101 (2015) 149–158. doi:10.1016/j.actamat.2015.08.018.

[49] J. Kim, C. Daniel Marioara, R. Holmestad, E. Kobayashi, T. Sato, Effects of Cu and Ag additions on age-hardening behavior during multi-step aging in Al-Mg-Si alloys, Materials Science and Engineering: A. 560 (2013) 154–162. doi:https://doi.org/10.1016/j.msea.2012.09.051.

[50] E.A. Mørtsell, C.D. Marioara, S.J. Andersen, J. Røyset, O. Reiso, R. Holmestad, Effects of Germanium, Copper, and Silver Substitutions on Hardness and Microstructure in Lean Al-Mg-Si Alloys, Metallurgical and Materials Transactions A. 46 (2015) 4369–4379. doi:10.1007/s11661-015-3039-5.

[51] S. Pogatscher, H. Antrekowitsch, M. Werinos, F. Moszner, S.S.A. Gerstl, M.F. Francis, et al., Diffusion on Demand to Control Precipitation Aging: Application to Al-Mg-Si Alloys, Physical Review Letters. 112 (2014) 225701. doi:10.1103/PhysRevLett.112.225701.

[52] E. Holmes, B. Noble, Resistivity examination of artficial ageing in an aluminium-copper-cadmium alloy, Journal of the Institute of Metals. 95 (1967) 106–110.

[53] B. Noble, Theta-prime precipitation in aluminium-copper-cadmium alloys, Acta Metallurgica. 16 (1968) 393–401. doi:10.1016/0001-6160(68)90026-6.

[54] J.D. Boyd, R.B. Nicholson, A calorimetric determination of precipitate interfacial energies in two Al-Cu alloys, Acta Metallurgica. 19 (1971) 1101–1109. doi:10.1016/0001-6160(71)90042-3.

[55] R. Sankaran, C. Laird, Effect of trace additions Cd, In and Sn on the interfacial structure and kinetics of growth of θ′ plates in Al-Cu alloy, Materials Science and Engineering. 14 (1974) 271 – 279. doi:10.1016/0025-5416(74)90108-6.

[56] J. Silcock, H. Flower, Comments on a comparison of early and recent work on the effect of trace additions of Cd, In, or Sn on nucleation and growth of θ′ in Al – Cu alloys, Scripta Materialia. 46 (2002) 389 – 394. doi:10.1016/S1359-6462(02)00003-9.

[57] D. Mitlin, J.W. Morris, V. Radmilovic, U. Dahmen, Precipitation and aging in Al-Si-Ge-Cu, Metallurgical and Materials Transactions A. 32 (2001) 197–199. doi:10.1007/s11661-998-0335-3.

[58] D. Mitlin, V. Radmilovic, U. Dahmen, J.W. Morris, On the influence of Si-Ge additions on the aging response of Al-Cu, Metallurgical and Materials Transactions A. 34 (2003) 735–742. doi:10.1007/s11661-003-0108-y.

[59] Y. Zhang, Z. Zhang, N. V. Medhekar, L. Bourgeois, Vacancy-tuned precipitation pathways in Al-1.7 Cu-0.025In-0.025Sb (at.%) alloy, Acta Materialia. 141 (2017) 341–351. doi:10.1016/J.ACTAMAT.2017.09.025.

[60] L. Bourgeois, C. Dwyer, M. Weyland, J.-F. Nie, B.C. Muddle, The magic thicknesses of θ′ precipitates in Sn-microalloyed Al – Cu, Acta Materialia. 60 (2012) 633 – 644. doi:10.1016/j.actamat.2011.10.015.

[61] E.E. Underwood, Quantitative Stereology, Addison-Wesley, 1970.

[62] Y. Zeng, S. Mu, P. Wu, K.P. Ong, J. Zhang, Relative effects of all chemical elements on the electrical conductivity of metal and alloys: An alternative to Norbury–Linde rule, Journal of Alloys and Compounds. 478 (2009) 345–354. doi:10.1016/j.jallcom.2008.11.035.

[63] Y.J. Li, L. Arnberg, Solidification structure of DC-cast AA3003 alloy and its influence on homogenization, Aluminium. 78 (2002) 834.

[64] M.F. Ashby, Oxide dispersion strengthening, in: AIME Conference Proceedings, New York, 1966: p. 143.

[65] Thermodynamic database, TCAL4-TCS Al-based alloy database, Version 4.0, Thermo-Calc software, (n.d.). www.thermocalc.com.

[66] W.B. Alexander, L.M. Slifkin, Diffusion of Solutes in Aluminum and Dilute Aluminum Alloys, Physical Review B. 1 (1970) 3274–3282. doi:10.1103/PhysRevB.1.3274.

[67] Y. Du, Y.. Chang, B. Huang, W. Gong, Z. Jin, H. Xu, et al., Diffusion coefficients of some solutes in fcc and liquid Al: critical evaluation and correlation, Materials Science and Engineering: A. 363 (2003) 140–151. doi:10.1016/S0921-5093(03)00624-5.

[68] D. Simonovic, M.H.F. Sluiter, Impurity diffusion activation energies in Al from first principles, Physical Review B. 79 (2009) 054304. doi:10.1103/PhysRevB.79.054304.

Tables

Table 1 Chemical compositions (wt. %) of the investigated alloys

Alloy	Mn	Fe	Si	Cd	Al
3003	1.15	0.58	0.20	-	bal.
3003_0.2Cd	1.10	0.50	0.18	0.21	bal.

Table 2 Mechanical properties of the 3003 and 3003_0.2Cd alloys subjected to different heat treatments

Samples	EC (MS/m)	YS (MPa)	UTS (MPa)	TE (%)
3003_0.2Cd, 450°C	22.8 ± 0.1	86 ± 1	136 ± 2	17.7 ± 0.6
3003, 450 °C	22.3 ± 0.1	69 ± 2	128 ± 2	25.9 ± 2.1
3003_0.2Cd, 600 °C_24h	22.1 ± 0.1	49 ± 1	126 ± 1	25.8 ± 0.4

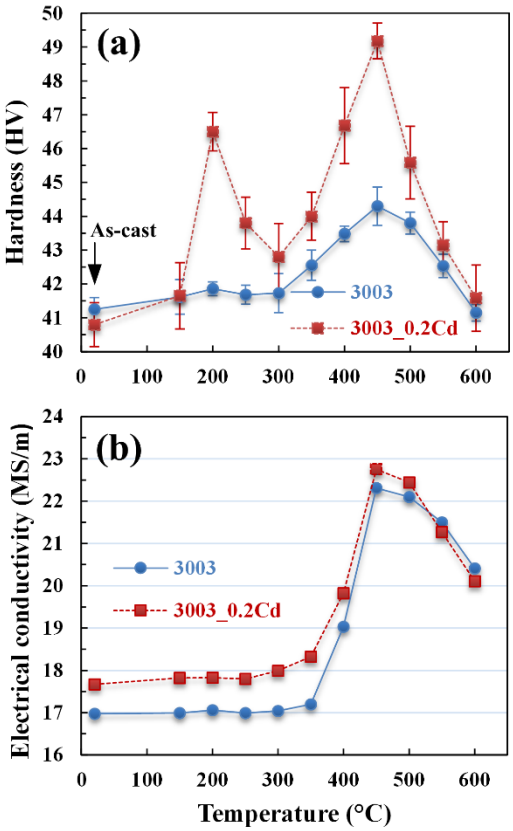

Figure 1 Evolution of (a) Vickers hardness and (b) EC of the 3003 and 3003_0.2Cd alloys during heating from RT to 600 °C at a rate of 50 °C/h. The increase of EC is an indication of the precipitation of Mn-rich α-Al(Mn,Fe)Si dispersoids while a decrease of EC means the dissolution of dispersoids.

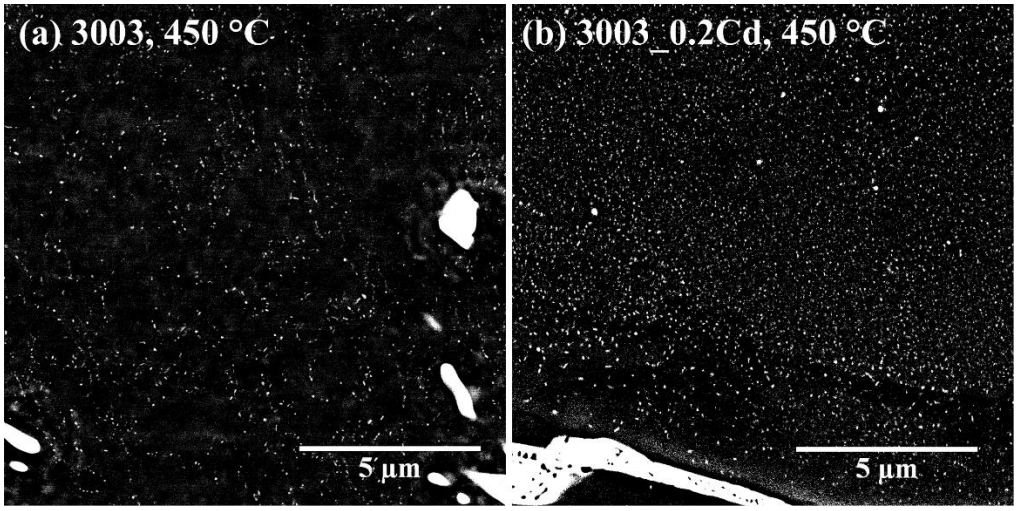

Figure 2 SEM micrographs of (a) 3003 and (b) 3003_0.2Cd alloys as-heated to 450 °C with dispersoids.

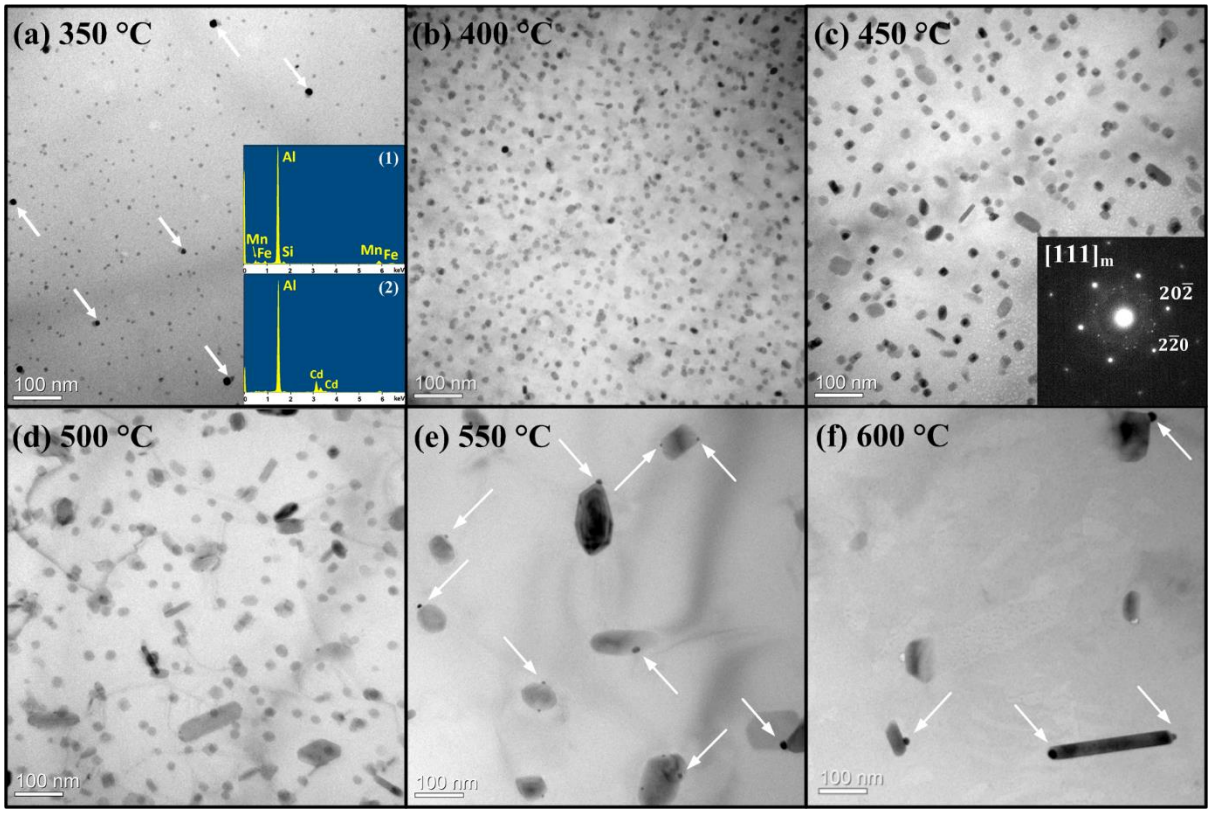

Figure 3 TEM micrographs of dispersoids in the 3003_0.2Cd alloy at (a) 350 °C; (b) 400 °C; (c) 450 °C; (d) 500 °C; (e) 550 °C and (f) 600 °C. White arrows indicate the unknown nanoparticles attached to dispersoids. All the presented images are taken at the regions with the densest dispersoids.

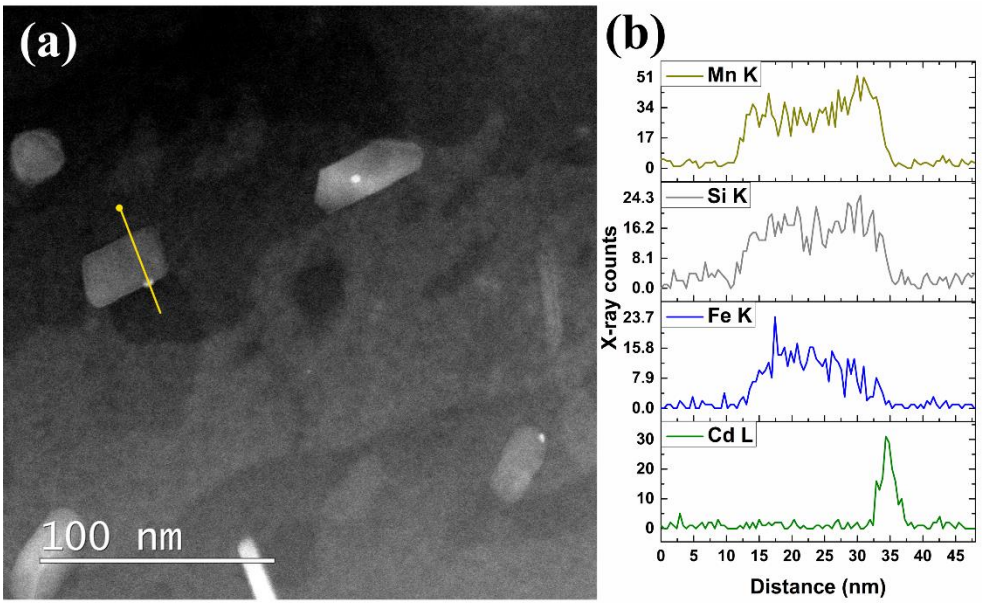

Figure 4 (a) HAADF-STEM image of dispersoids in the 3003_0.2Cd alloy as-heated to 450 °C and (b) corresponding EDS line profile of one particle indicated in (a). The STEM-EDS result confirms that the dispersoid is α-Al(Mn,Fe)Si phase and the bright particle attached to the dispersoid is a Cd-rich nanoparticle.

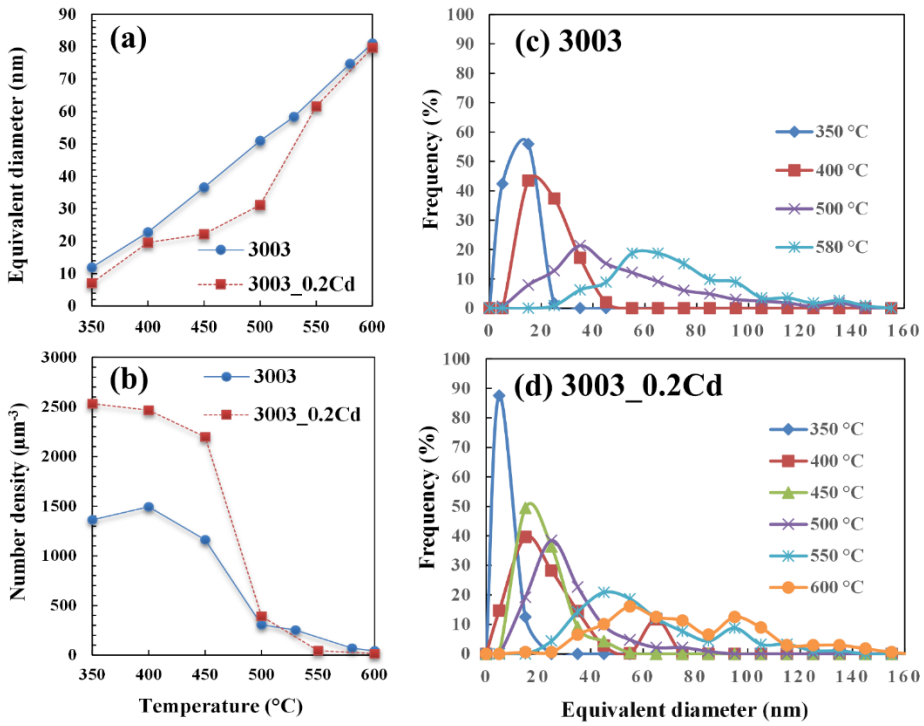

Figure 5 (a) Equivalent diameter and (b) number density of dispersoids during heating between 350 and 600 °C; size distribution of dispersoids during heating in (c) 3003 alloy [38] *and (d) 3003_0.2Cd alloy.*

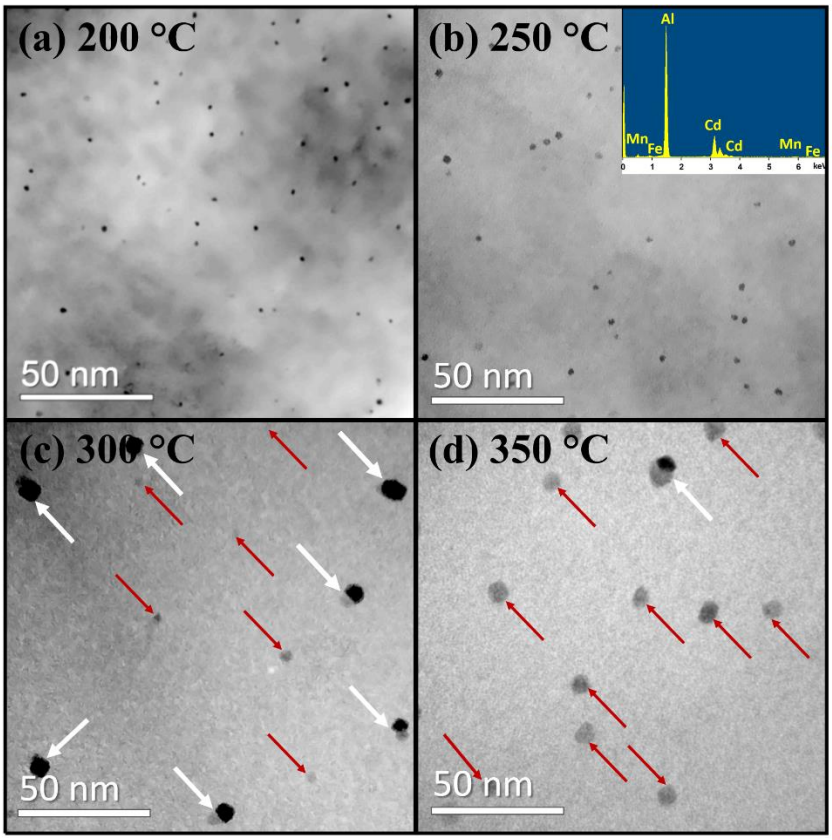

Figure 6 TEM micrographs of the 3003_0.2Cd alloy as-heated to (a) 200 °C; (b) 250 °C; (c) 300 °C and (d) 350 °C. White arrows indicate the "composite" nanoparticles, and red arrows indicate individual dark grey dispersoids.

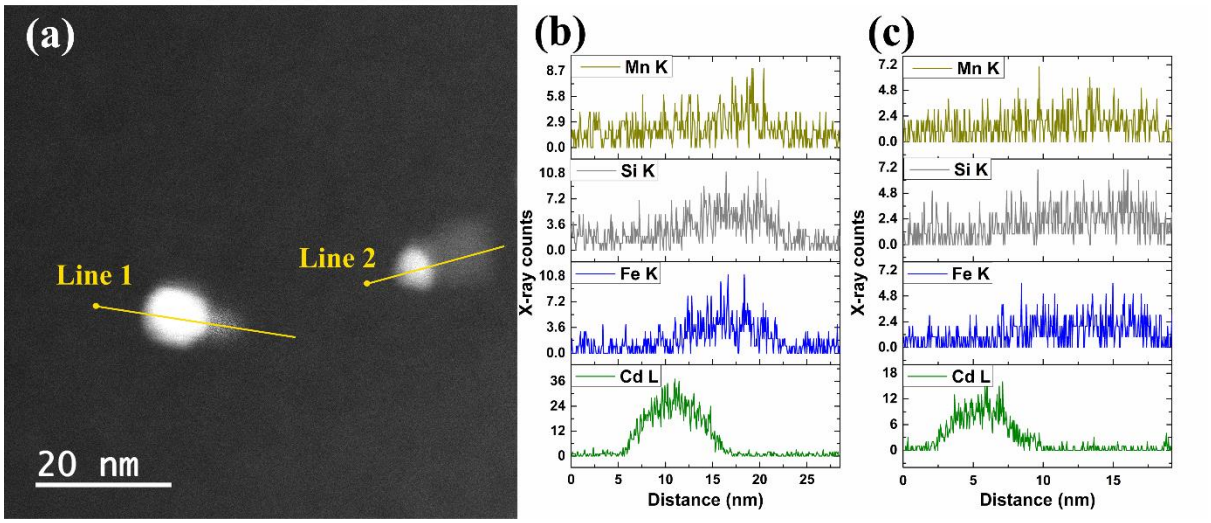

Figure 7 (a) HAADF-STEM image of nanoparticles in the 3003_0.2Cd alloy as-heated to 300 °C and corresponding EDS line profiles of (b) line 1 and (c) line 2. EDS analyses reveal that the "composite" nanoparticles is highly likely to comprise one Cd-rich particle and one α-Al(Mn,Fe)Si dispersoid.

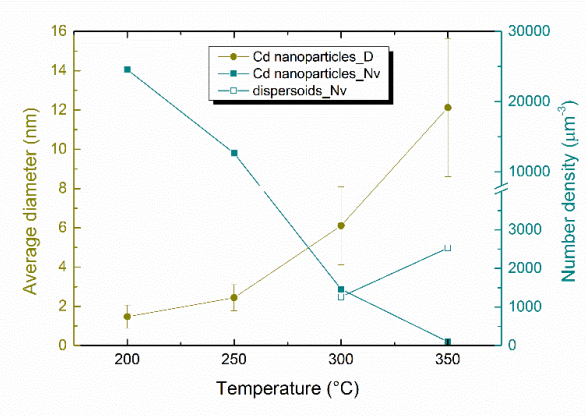

Figure 8 The average diameter (D) and number density (Nv) of Cd-rich nanoparticles and dispersoids in the 3003_0.2Cd alloy at 200-350 °C. Note that the displayed number density of dispersoids at 300 °C is based on the measurement of independent dispersoids observed and does not take into account the attached dispersoids in "composite" particles.

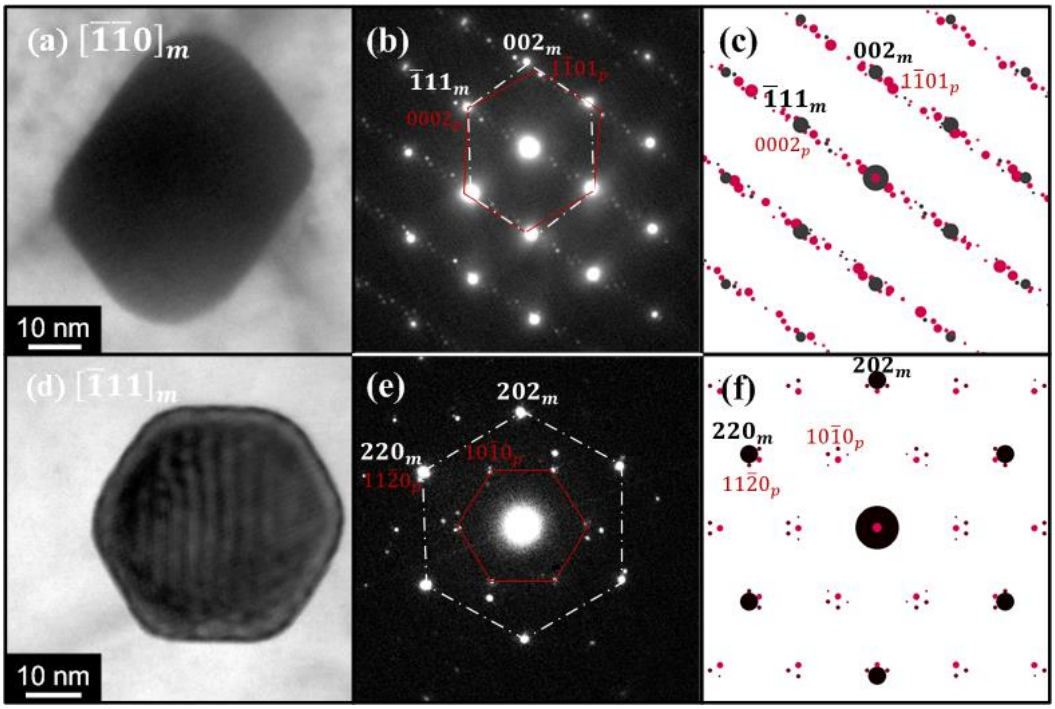

Figure 9 Bright-field TEM images of coarse Cd-rich nanoparticles in the 3003_0.2Cd alloys as-heated to 250 and 300 °C along (a) $[\bar{1}\bar{1}0]_m$ *and (d)* $[\bar{1}11]_m$ *zone axes and the corresponding SAED patterns in (b) and (e), respectively. The right column is the simulated double diffraction patterns of dispersoids and the Al matrix along (c)* $[\bar{1}\bar{1}0]_m$ *and (f)* $[\bar{1}11]_m$ *zone axes, respectively, assuming that the orientation relationship between hcp Cd phase and α-Al matrix is* $(11\bar{2}0)_p \parallel (220)_m, [0001]_p \parallel [\bar{1}11]_m$.

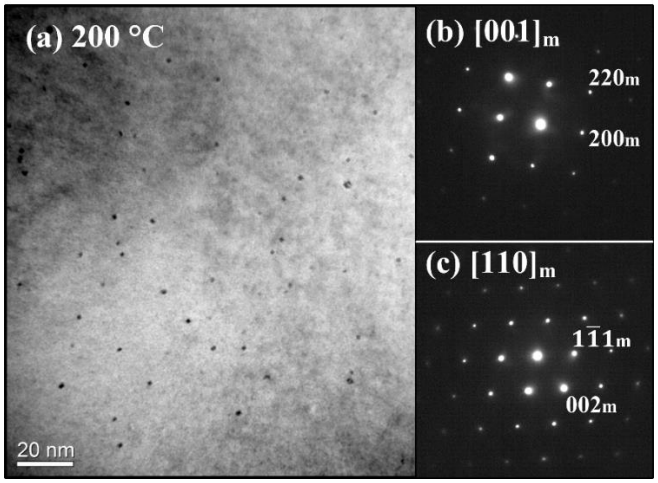

Figure 10 (a) Bright-field TEM image of Cd-rich nanoparticles formed at 200 °C and SAED patterns along (b) [001] *and (c)* [110] *zone axes (multiple Cd-rich nanoparticles are included). No extra diffraction spot except for the diffraction patterns of α-Al can be observed.*

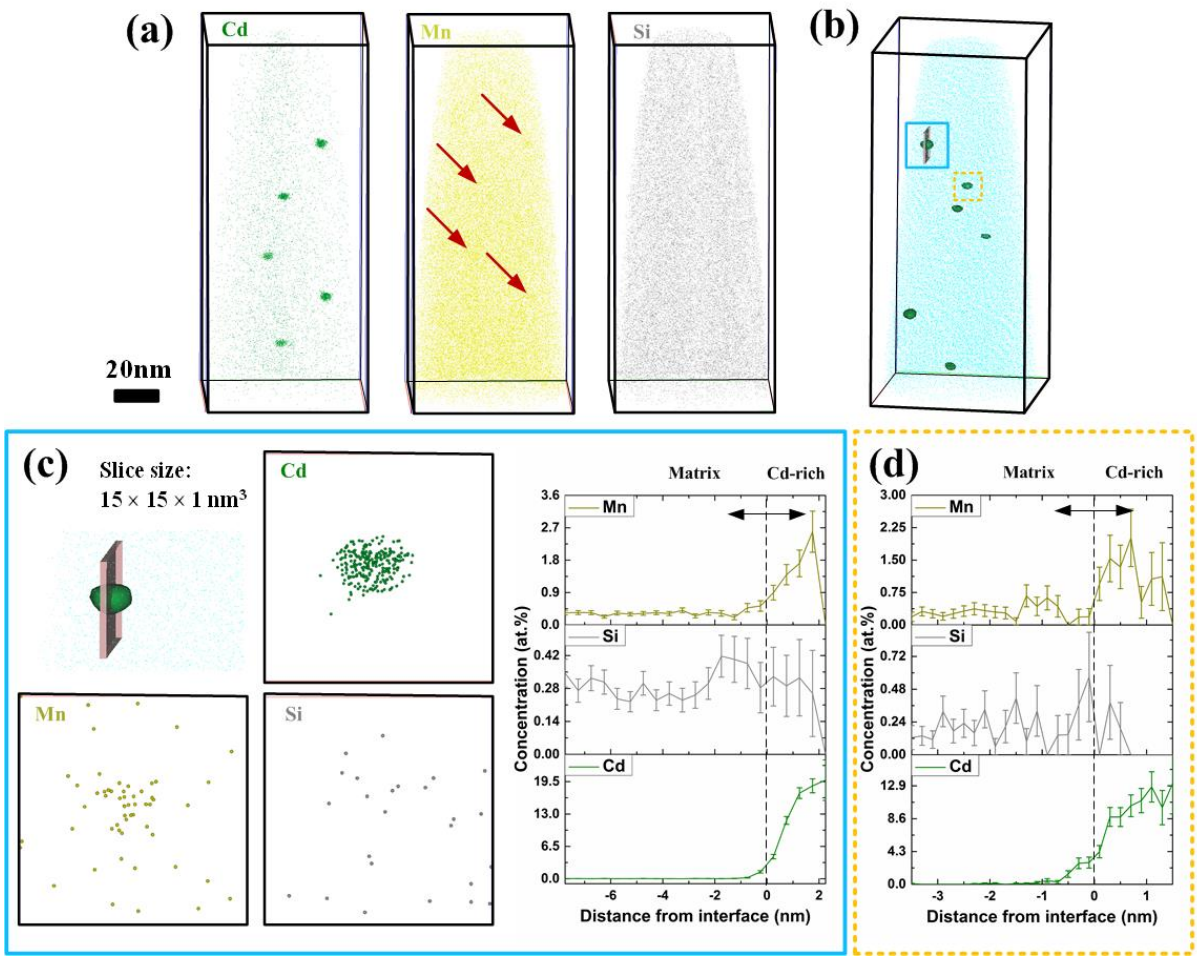

Figure 11 APT results of the 3003_0.2Cd alloy as-heated to 250 °C. (a) Three-dimensional reconstruction of Cd (green), Mn (yellow) and Si (grey) atoms within the selected volume; (b) Isosurfaces (green) for regions with higher than 4.6 at.% Cd; (c) atom distributions in/around the Cd-rich particle in the blue box in (b) and proxigram profile showing the distributions of Mn, Si and Cd in/around Cd-rich nanoparticles. (d) proxigram profile of another Cd-rich nanoparticle in the orange dashed box in (b).

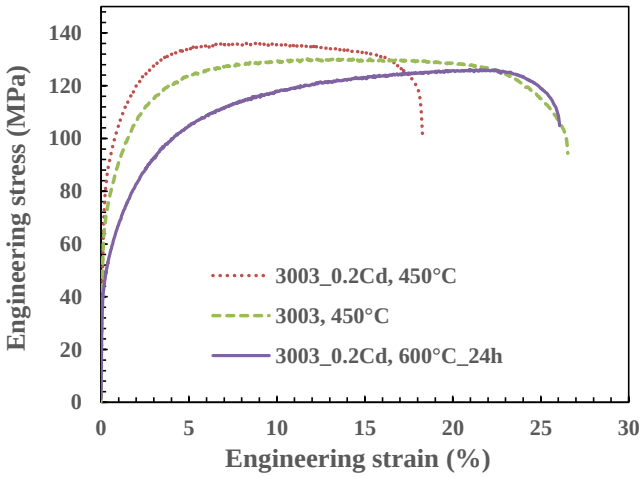

Figure 12 Engineering stress-strain curves of the 3003 and 3003_0.2Cd alloys as-heated to 450 °C. The tensile curve of the 3003_0.2Cd alloy homogenized at 600 °C for 24h is displayed for comparison, where the dispersoids have dissolved and the solute concentration of Mn is nearly the same as the investigated two alloys as-heated to 450°C.

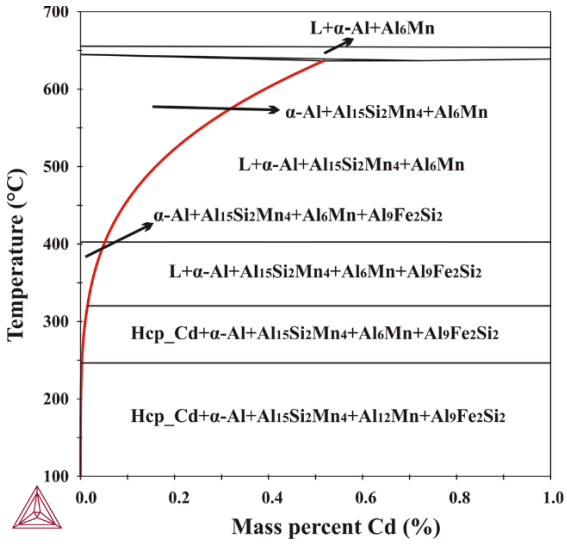

Figure 13 Calculated phase diagram showing the solubility of Cd (red) of the Al matrix in a 3003 alloy (Al-1.1Mn-0.5Fe-0.18Si) as a funcotion of temperature. In the phase diagram, L is liquid.